



Cite this: *Nanoscale*, 2015, 7, 11409

The influence of flow, shear stress and adhesion molecule targeting on gold nanoparticle uptake in human endothelial cells†

Henrik Klingberg,^{a,b} Steffen Loft,^a Lene B. Oddershede^b and Peter Møller*^a

The uptake of nanoparticles by endothelial cells is dependent on shear stress adaptation and flow exposure conditions. Adaptation of primary human umbilical vein endothelial cells (HUVECs) to shear stress for 24 h was associated with reduced internalisation of unmodified 80 nm spherical gold nanoparticles (AuNPs) (mean hydrodynamic size of 99 nm in culture medium) after exposure to flow conditions compared with cells that were cultured and exposed to static conditions. Under static conditions, targeting of 80 nm AuNPs conjugated with antibodies against the intracellular adhesion molecule 1 (ICAM-1) (mean hydrodynamic size of 109 nm in culture medium) markedly increased the internalisation of AuNPs in HUVECs that were activated with the tumour necrosis factor (TNF), a treatment that markedly increased the surface expression of ICAM-1. Shear stress-adapted and TNF-activated HUVECs, which were exposed to flow conditions, had higher association with anti-ICAM-1 AuNPs than cells that were not TNF-activated or exposed to particles under static conditions. Hence, shear stress adaptation reduces the uptake of unmodified AuNPs and increases the association between anti-ICAM-1 AuNPs and TNF-activated HUVECs.

Received 6th March 2015,
Accepted 21st May 2015

DOI: 10.1039/c5nr01467k

www.rsc.org/nanoscale

Introduction

The interaction between nanoparticles (NPs) and endothelial cells is highly relevant for nanomedicine-candidates because the endothelium constitutes the main barrier between the blood flow and the adjacent tissue.¹ Repetitive mechanical deformation of vessel walls (*i.e.*, cyclic strain) is an important modulator of the vascular cell function.² In addition, the blood flow promotes a directional force on the vessel wall, resulting in shear stress, which depends on the blood viscosity, flow rate, and the vessel radius and elasticity.^{2–5} Shear stress is known to promote cytoskeletal reorganisation, including the pronounced formation of dense F-actin stress fibres in primary human umbilical vein endothelial cells (HUVECs).⁶ Furthermore, microarray analyses have documented altered expression of a large number of genes in endothelial cells cultured in shear stress compared with cells cultured under static conditions.^{7,8} The effects of shear stress on NP-uptake play an

important role in the application of nanomedicine designated for intravenous delivery, since the particle–cell interaction is affected by flow dynamics.⁹ Targeting of drugs to specific tissues by the use of engineered nanocarriers is one of the principle applications of nanomedicine.¹⁰ Recently, the targeting of anti-inflammatory nanomedicine has received increasing interest.¹¹ Extravasation of leukocytes is the hallmark of inflammation, which is initiated by the activation of endothelial cells, the activation increases surface expression of adhesion molecules, which assists the migration through the endothelium.¹² The activation of endothelial cells by the tumour necrosis factor (TNF) increases the levels of CD54 also known as intercellular adhesion molecule 1 (ICAM-1) cell surface expression.¹³ NPs conjugated with full length anti-ICAM-1 immunoglobulin G antibodies have been successfully targeted and internalised by activated endothelial cells both in cell cultures and animals.^{14–16} Several studies on effects of shear stress on anti-ICAM-1 NPs and cell associations have been performed on HUVECs and mouse brain endothelioma (bEnd.5) cells.^{17–20} The particles used were either polystyrene or liposomes and all experiments showed unaltered or reduced association between anti-ICAM-1-NPs and cells when exposed to flow conditions compared with the static control. These studies used NPs that were conjugated with the full-length anti-ICAM-1 antibodies by simple adsorption. However, using cleaved rather than full-length antibodies has shown to

^aDepartment of Public Health, Section of Environment Health, University of Copenhagen, Øster Farimagsgade 5B, DK-1014 Copenhagen, Denmark.
E-mail: pemo@sund.ku.dk

^bNiels Bohr Institute, University of Copenhagen, Blegdamsvej 17, DK-2100 Copenhagen, Denmark

†Electronic supplementary information (ESI) available. See DOI: 10.1039/c5nr01467k

increase the stability of conjugation to gold surfaces.²¹ Gold nanoparticles (AuNPs) have been extensively used in the development of nanomedicine as a model, drug, or diagnostic NP.^{22–25}

We have investigated the effects of shear stress adaptation and flow exposure conditions on the uptake of unmodified and ICAM-1 targeted AuNPs in HUVECs. The cells were either cultured under static conditions or adapted to shear stress under flow conditions for 24 h prior to AuNP-exposure under static or flow conditions. Furthermore, we investigated targeting and uptake of AuNPs conjugated with cleaved anti-ICAM-1 antibodies in TNF-activated HUVECs under both static and flow conditions.

Experimental

For detailed method descriptions see the ESI.†

Cell culture

HUVECs were obtained from Gibco (NY, USA) and cultured in supplemented endothelial growth medium with 2% foetal bovine serum (Cell Applications Inc., San Diego, CA, USA). All culture surfaces were coated with EmbryoMax® 0.1% Gelatin Solution (Merck Millipore, Darmstadt, Germany) for 30 min prior to cell seeding. The HUVECs were activated by exposure to 10 ng ml⁻¹ of TNF for 24 h prior to AuNP exposure (ESI Fig. S1 and S2† describe the concentration–response relationship and its effect on the cell size and granularity).

Shear stress and flow system

Prior to AuNP exposure HUVECs were either cultured under static conditions without flow (termed *non-adapted* cells) or under 10 dyn flow conditions for 24 h (termed *shear stress adapted* cells). The exposure to AuNPs was carried out either under static conditions without flow (termed *static exposed* cells) or under 10 dyn flow conditions (termed *flow exposed* cells). HUVECs were seeded in Ibidi µSlides VI^{0.4} (Ibidi, Planegg, Germany) multichannel flow chambers (3 × 10⁴ per flow channel) four days prior to AuNP exposure.

The flow system was set up with parallel flow-loops each connected to one flow channel (Fig. 1). The flow system was placed in a cell culture incubator with an external multi-channel peristaltic pump (Watson Marlow Pumps, Falmouth, UK). The pump and tubing outside of the incubator was heated and insulated to maintain a constant temperature of 37 °C. A low gas permeable PharmaPure® pump tubing (Saint-Gobain Performance Plastics, Charny, France) was used together with a low gas permeable PharMed® BPT tubing (Saint-Gobain) outside the incubator. For the remaining tubing running inside the incubator (5% CO₂ and 95% humidity), a high gas permeable platinum-coated Tygon® silicon tubing was used (Saint-Gobain). The reservoirs and bubble traps were obtained from DTU Systems Biology (described by Tolker-Nielsen and Sternberg²⁶) with a custom made inner diameter of 1.6 mm to fit the flow system. Five ml syringes were used as reservoirs (Terumo, Elkton, USA) and sterile lids

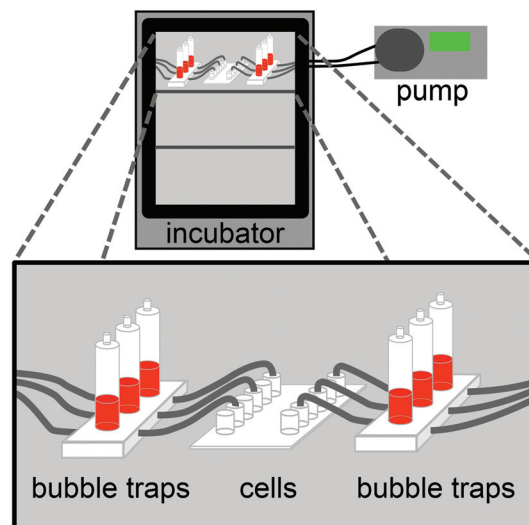


Fig. 1 Experimental setup for flow conditions. Flow loops with cell growth medium directed by an external peristaltic pump, feeding the first bubble traps, followed by the cell culture flow-chambers and the second bubble traps before returning the medium to the pump.

matching the syringe Luer connectors were used. The pump flow rate was measured before each experiment.

Antibody fragmentation

The monoclonal mouse anti-human CD54 (ICAM-1) IgG1 LEAF™ (low endotoxin and azide-free) purified antibody was obtained from BioLegend® (San Diego, CA, USA). To obtain half immunoglobulin G1 (IgG1) fragments, the anti-ICAM-1 antibody was incubated in 0.1 M phosphate buffer (pH 6) containing ethylenediaminetetraacetic acid (EDTA, Sigma Aldrich, St. Louis, MO, USA) and mercaptoethylamine (2-MEA, Sigma-Aldrich) at 37 °C for 1.5 h and 3 h. The sub 7 kDa compounds were removed by running the sample twice through a Zeba Spin Desalting Column (Thermo Fisher Scientific Inc., Rochester, NY, USA) with a EDTA containing Tris (pH 8) buffer. The solution was stored at 4 °C and used within a few days.

SDS-PAGE and Coomassie blue staining

The 2-MEA treated and untreated mouse anti-ICAM-1 antibodies were analysed by SDS-PAGE and Coomassie blue staining to check the amount of cleaved antibodies. The loading buffer was prepared without β-mercaptoethanol to ensure that the antibodies were unaffected by the buffer.

AuNP modification

Colloidal spherical AuNPs Ø 80 nm (coefficient of variation <8% according to the manufacturer) were obtained from BBI Solutions (Cardiff, UK). The intact or cleaved antibodies were conjugated with the AuNPs by the addition of the intact or cleaved antibodies to the AuNP stock solution at a final concentration of 123 ng protein per µg AuNPs. For conjugation with cleaved antibodies the anti-ICAM-1 antibodies were incubated for 3 h with 2-MEA.

Nanoparticle characterisation

Hydrodynamic size-distribution, stability and precipitation of anti-ICAM-1 AuNPs were compared with unmodified AuNPs re-suspended in ddH₂O and supplemented endothelial growth medium by LM20 NanoSight (Salisbury, UK) and NanoSight Nanoparticle Tracking Analysis (NTA v. 3.0) and UV-Vis spectroscopy (Shimadzu, Kyoto, Japan).

AuNP exposure

The AuNPs were centrifuged and re-suspended in the endothelial growth medium. The AuNP exposure concentration used throughout this work was 5 µg ml⁻¹ which corresponds to 25.4 µM, 9.67 × 10⁸ particles per ml and a total surface area of 0.19 cm² ml⁻¹. The AuNP exposure time used throughout this work was 3 h followed by extensive wash. In previous work, we have shown that concentrations up to 50 µg ml⁻¹ of AuNPs were not associated with increased cytotoxicity, assessed by cellular succinate dehydrogenase activity (WST-1 assay) and cell count (Calcein-AM staining).²⁷

Confocal microscopy

HUVECs were seeded in Ibidi µSlides VI^{0.4} multichannel flow chambers (3 × 10⁴ cells per flow channel) four days prior to AuNP exposure. Just prior to fixation, cells were stained with CellTracker™ Green CMFDA (20 µM) (Molecular Probes®, Eugene, OR, USA). Cells were fixed in 4% paraformaldehyde and mounted with Ibidi mounting medium (Ibidi). Images were collected on a Leica SP5 confocal microscope (Leica Microsystems, Mannheim, Germany) using a 100× magnification Leica NA: 1.42, oil immersion objective (Leica Microsystems). CellTracker Green was excited at λ 488 nm and emission was collected at λ 510–550 nm. AuNPs were visualised in reflection mode with a HeNe laser at λ 633 nm laser (collected at λ 631–636 nm). The AuNP uptake analysis was performed as described by Klingberg *et al.*²⁷ The ratio between the cell volume (CellTracker Green) and the relative AuNP volume was then calculated. The volume corresponds to the signal volume and not the actual volume of the AuNPs since the sizes of 80 nm AuNPs are well below the diffraction limit of light. F-actin was stained with (1 : 100) rhodamin phalloidin (Molecular Probes) and the nucleus with Hoechst 33342 (Molecular Probes). Rhodamin phalloidin was excited at λ 543 nm and emission was collected at λ 551–606 nm and Hoechst was excited at λ 406 nm and emission was collected at λ 428–464 nm.

Flow cytometry

We used flow cytometry for AuNP-uptake quantification in the present study because it was designed to assess relative differences in uptake between exposure conditions. In a previous study on the same type of AuNP material, we obtained an excellent consistency in the quantification of AuNPs in HUVECs by flow cytometry, 3D confocal microscopy and single particle ICP-MS.²⁷ Samples were analysed on a flow cytometer BD Accuri™ C6 Flow Cytometer (Becton, Dickinson and

Company (BD), Franklin Lakes, NY, USA). HUVECs were seeded (1 × 10⁵ cells per well) in Nunc™ 12 well plates (Nunc, Roskilde, Denmark) one day prior to AuNP-exposure. For AuNP uptake and ICAM-1 and PECAM-1 expression experiments HUVECs were seeded as for confocal microscopy experiments. Cells were detached using Accutase™ Cell Detachment Solution (BD). The cells were stained with antibodies against ICAM-1 (R-phycoerythrin (PE) mouse anti-human CD54, BD) and PECAM-1 (fluorescein isothiocyanate (FITC) mouse anti-human CD31, BD). The measurement of PECAM-1 was included to compare the ICAM-1 response to a differently regulated cell adhesion protein on HUVECs. The exposure to TNF has been shown to down-regulate the surface expression of PECAM-1, whereas ICAM-1 is up-regulated.²⁸

Statistical analysis

Statistical significances were assessed by linear regression analysis and ANOVA tests. The *P* < 0.05 level was accepted as the statistical significance level. The statistical analyses were performed using OriginPro 9.0 (Origin Lab Corporation, Northampton, MA, USA).

Results

Particle characterisation

The hydrodynamic size-distributions of unmodified AuNPs (AuCtrl), intact anti-ICAM-1 antibody conjugated AuNPs (AuAb) and cleaved anti-ICAM-1 antibody conjugated AuNPs (Au^{1/2}Ab) were analysed by NanoSight Brownian motion video analysis (Table 1). The hydrodynamic mean size of both AuAb and Au^{1/2}Ab increased as compared with AuCtrl after re-suspension in either water or serum-containing endothelial medium (*P* < 0.001, *P* < 0.02, respectively). The mean hydrodynamic sizes of AuCtrl, AuAb and Au^{1/2}Ab were also increased when re-suspended in HUVEC medium as compared with water (*P* < 0.001 for all particles). Similar results were obtained for the mode of the size-distribution. No significant changes in the absorption/extinction peak wavelength and height were observed between AuCtrl, AuAb and Au^{1/2}Ab by UV-Vis, indicating that no significant precipitation of the AuNPs had occurred during the AuNP conjugation (size-distribution histograms are shown in Fig. S3 in the ESI†).

SDS-PAGE and Coomassie blue staining

The efficiency of the anti-ICAM-1 antibody cleavage by 2-MEA was examined by SDS-PAGE gel electrophoresis and subsequent Coomassie blue staining. The yield of the antibody cleavage was 45% cleaved protein and 55% intact protein after 3 h incubation with 10.5 mM 2-MEA (Fig. S4 in the ESI†).

Effect of shear stress adaptation and flow exposure on the morphology of HUVECs

To determine the effect of shear stress adaptation and flow exposure on the internalisation of unmodified AuNPs (AuCtrl) by HUVECs, cells were either cultured under static conditions

Table 1 Hydrodynamic size of AuNPs with or without anti-ICAM-1 surface modifications. Brownian motion analysis of AuNPs suspended in H₂O or supplemented endothelial growth medium containing 2% serum (medium). The AuNPs were either unmodified (AuCtrl), conjugated with intact anti-ICAM-1 antibodies (AuAb) or conjugated with cleaved anti-ICAM-1 antibodies (Au $\frac{1}{2}$ Ab). The results are averages and standard deviations (SD) of 20 measurements made on 4 different days (15 measurements made on 3 different days for Au $\frac{1}{2}$ Ab)

Particle and re-suspension	AuCtrl H ₂ O	AuAb H ₂ O	Au $\frac{1}{2}$ Ab H ₂ O	AuCtrl medium	AuAb medium	Au $\frac{1}{2}$ Ab medium
Mean size \pm SD (nm)	82.6 \pm 3.9	88.2 \pm 4.9	87.2 \pm 2.3	98.8 \pm 2.9	108.9 \pm 12.4	109 \pm 9.9
Mode \pm SD (nm)	86.5 \pm 3.1	90 \pm 4.2	89.5 \pm 2.9	99.4 \pm 3.1	102.6 \pm 3.9	104.3 \pm 4.3

(non-adapted) or under flow conditions for 24 h (10 dyn) (shear stress adapted) prior to AuNP exposure for 3 h (5 $\mu\text{g ml}^{-1}$) either under static (static exposed) or under flow conditions (flow exposed). HUVECs were stained with rhodamin phalloidin to visualise the actin skeleton (F-actin) in order to examine shear stress related changes of the cytoskeleton. Both shear stress adapted cells and flow exposed cells showed the formation of dense actin stress fibres (Fig. S5[†]). We did not observe any clear change in F-actin organisation related to the AuNP exposure (both for non-adapted and shear stress adapted cells). The shear stress adapted cells and to a lesser degree flow exposed cells were associated with reduced Cell-Tracker Green staining compared with non-adapted and static exposed cells.

Cellular uptake of unmodified AuNPs under shear stress adaptation and flow conditions

AuNP-uptake was analysed by CLSM and 3D image volume measurement analysis (Fig. 2). Non-adapted and flow exposed HUVECs had a slightly reduced internalisation of AuCtrl compared with static exposed cells ($P = 0.10$). A similar reduction in AuNP internalisation was observed for shear stress adapted and static exposed cells ($P = 0.23$). The most pronounced reduction in AuNP internalisation was observed in shear stress adapted and flow exposed cells; these cells had lower AuCtrl internalisation compared with any of the other groups ($P < 0.05$). Confocal 3D images showed that only a negligible fraction of the observed AuCtrl was localised in what appeared to

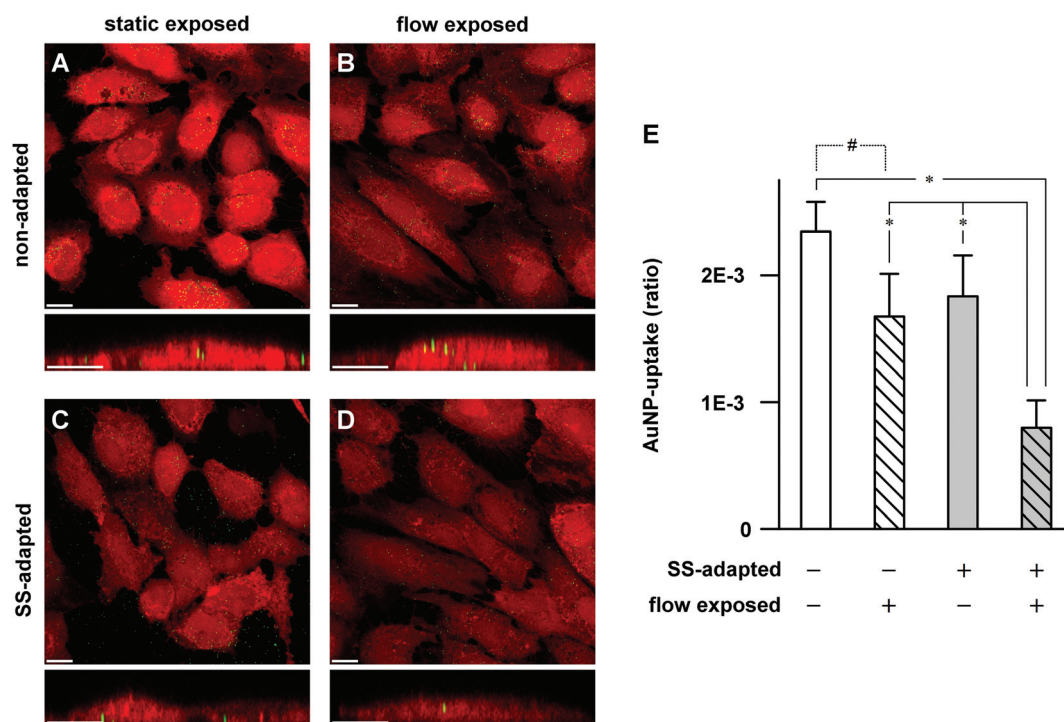


Fig. 2 The effect of shear stress (SS) adaptation and flow exposure conditions for gold nanoparticle (AuNP) uptake by HUVECs. SS adapted cells were cultured under flow conditions with 10 dyn shear stress for 24 h prior to 3 h AuNP exposure (5 $\mu\text{g ml}^{-1}$) under either static or flow conditions (10 dyn). Panels A–D show representative images of image-stacks used for AuNP-uptake analysis. Each panel shows an extended focus image (top; scale bar = 14 μm) and a cropped XZ image plane (bottom; scale bar = 5 μm). Panel E shows quantified AuNP uptake based on 3D CLSM data analysis, where the uptake (ratio) is determined by comparing the total cellular volume with the total overlapping relative volume of the AuNPs. Error bars represent means and SEMs of 5 (and 4 non-adapted and static-exposed cells) independent experiments, * $P < 0.05$, # $P = 0.10$.

be near or on the surface of the cells. Furthermore, the signal from AuCtrl, which was not overlapping with the signal from the stained cells, was excluded from the uptake quantification. Video documentation of 3D-imaging is provided in the ESI (files S1 and S2†).

AuNP modification with anti-ICAM-1 antibodies and cellular uptake

A high through-put comparative experiment was performed to determine the cellular targeting of anti-ICAM-1 antibody conjugated AuNPs of TNF-activated and non-activated HUVECs and the effect of antibody cleavage on this targeting. This was performed under static exposure conditions and measured by flow cytometry and SSC-A analysis (Fig. 3). Cells were grown on 12-well culture plates. There was a statistically significant interaction between the TNF-activation and AuNP exposure ($P < 0.001$).

The increase in SSC-A was significant for all types of AuNPs ($P < 0.001$) when compared with unexposed cells. A significant increase in SSC-A for unexposed TNF-activated cells compared with unexposed non-activated cells was also observed ($P < 0.05$). The increase in uptake of AuCtrl was borderline

significant for TNF-activated cells when compared with TNF-activated unexposed cells ($P = 0.053$). No significant increase in SSC-A was observed in non-activated cells exposed to both types of anti-ICAM-1 conjugated AuNPs (AuAb and Au $\frac{1}{2}$ Ab) compared with AuCtrl. A highly significant increase in SSC-A was observed for TNF-activated cells exposed to AuAb and Au $\frac{1}{2}$ Ab compared with their respective non-activated exposure controls and TNF-activated and non-activated cells exposed to AuCtrl ($P < 0.001$). We chose to use Au $\frac{1}{2}$ Ab in further experiments due to the stronger binding of the exposed thiol-group on the cleaved IgG heavy chain as compared with the unspecific conjugation of the intact antibody on AuAb.

Confocal image analysis of cellular uptake of anti-ICAM-1 AuNPs

To assess the cellular localisation of the AuNPs and to directly compare the AuNP-uptake between TNF-activated and non-activated cells, the AuNP-uptake was quantified by CLSM and 3D image volume measurement analysis. The cells were cultured under static conditions in flow channels to be able to compare with flow exposure experiments. Visual inspection of the confocal 3D images indicated that the majority of both AuCtrl and Au $\frac{1}{2}$ Ab particles were mainly located in what appeared as small intracellular vesicular structures, whereas there were no particles found inside the nucleus and few particles were observed near or on the cellular surface (see Fig. S6 and S7 in the ESI†).

Using confocal microscopy, we quantified the uptake of AuCtrl and Au $\frac{1}{2}$ Ab in TNF-activated and non-activated HUVECs (Fig. 4). In accordance with the flow cytometry results (Fig. 3), a highly significant increase in the uptake of Au $\frac{1}{2}$ Ab was observed for TNF-activated cells compared with non-activated cells ($P < 0.001$). A significant increase in the uptake of Au $\frac{1}{2}$ Ab was also observed for non-activated cells as compared with the uptake of AuCtrl ($P < 0.05$). No significant change was observed for the uptake of AuCtrl in TNF-activated cells compared with non-activated cells. Since the exposure volumes varied from open 12-well culture plates to closed flow channels we also analysed cellular AuNP uptake for cells cultured in flow channels by flow cytometry analysis. Again we found enhanced uptake of Au $\frac{1}{2}$ Ab in TNF-activated cells, whereas no significant increased uptake of AuCtrl was observed for TNF-activated cells compared with unexposed non-activated and TNF-activated cells (Fig. S8 in the ESI†).

ICAM-1 cellular targeting in TNF-activated, shear stress adapted and flow exposed cells

HUVECs were TNF-activated and shear stress adapted for 24 h (10 dyn) prior to a 3 h exposure period to Au $\frac{1}{2}$ Ab (5 $\mu\text{g ml}^{-1}$) under flow conditions. As a reference condition, we used HUVECs that were not exposed to TNF or shear stress adapted, whereas they were exposed to Au $\frac{1}{2}$ Ab for 3 h under static conditions. Fig. 5 panel A shows a representative example of non-activated cells after static exposure to Au $\frac{1}{2}$ Ab. Panels B and C show a representative example of TNF-activated cells after static exposure to Au $\frac{1}{2}$ Ab. Panel D shows a representative

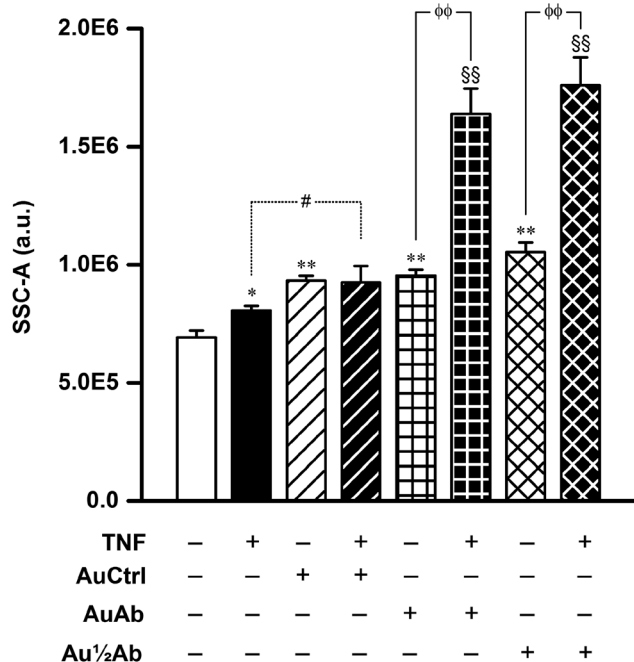


Fig. 3 Flow cytometry analysis of the cellular uptake of unmodified or anti-ICAM-1 gold nanoparticles (AuNPs) by non-activated or TNF-activated HUVECs under static conditions. Cells were non-activated (white) or activated by 24 h pre-incubation with 10 ng ml^{-1} TNF (black) followed by AuNP-exposure (5 $\mu\text{g ml}^{-1}$ for 3 h) under static conditions. The AuNPs were either unmodified (AuCtrl), conjugated with full size anti-ICAM-1 antibodies (AuAb) or conjugated with MEA-2 cleaved anti-ICAM-1 antibodies (Au $\frac{1}{2}$ Ab). * $P < 0.05$, ** $P < 0.001$ compared with the unexposed and non-activated cells. §§ $P < 0.001$ compared with unexposed that were TNF-activated. $\phi\phi P < 0.001$ and # $P = 0.053$. Error bars represent SEMs of 4 (3 for Au $\frac{1}{2}$ Ab – cleaved) independent experiments.

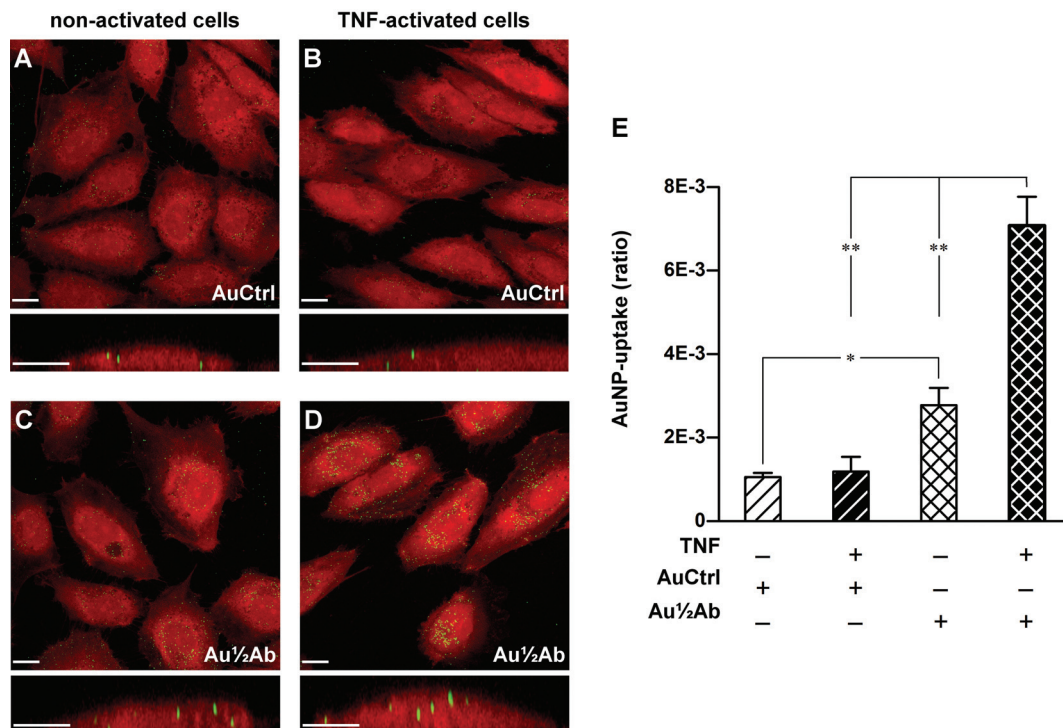


Fig. 4 Confocal microscopy analysis of the cellular uptake of unmodified or anti-ICAM-1 gold nanoparticles (AuNPs) by non-activated or TNF-activated HUVECs under static conditions. Cells were exposed to AuNPs for 3 h ($5 \mu\text{g ml}^{-1}$) and activated with TNF (10 ng ml^{-1}) 24 h prior to AuNP exposure. Panels A–D show representative examples of image-stacks used for relative AuNP-uptake quantification. Each panel shows an extended focus image (top; scale bar = $14 \mu\text{m}$) and a cropped XZ image plane (bottom; scale bar = $5 \mu\text{m}$). The cytoplasm was stained by CellTracker (red) and AuNPs were visualised by particle reflection (green). Cells were exposed to either unmodified AuNPs (AuCtrl) or cleaved anti-ICAM antibody-conjugated AuNPs (Au $\frac{1}{2}$ Ab). Panel E shows quantified data on the AuNP uptake based on 3D CLSM data analysis, where the uptake (ratio) is determined by comparing the total cellular volume with the total overlapping relative volume of the AuNPs. * $P < 0.05$, ** $P < 0.001$, error bars are SEMs of 5 (4 for control AuCtrl) independent experiments.

example of non-activated and shear stress adapted cells that were exposed to Au $\frac{1}{2}$ Ab under flow conditions. Panels E and F show a representative example of shear stress adapted and TNF-activated cells exposed to Au $\frac{1}{2}$ Ab under flow conditions. The exposure under flow conditions was associated with localisation of Au $\frac{1}{2}$ Ab to the cell surface rather than the cytosol. In contrast, both non-activated and TNF-activated cells that were exposed under static conditions showed Au $\frac{1}{2}$ Ab to be localised to intracellular compartments of the cells. Video documentation of 3D-imaging is provided in the ESI (files S3 and S4[†]). TNF-activated cells displayed a high association with Au $\frac{1}{2}$ Ab from what appears to be single or a few NPs to larger agglomerates (panels E and F).

The large formation of cell-surface agglomerates on TNF-activated HUVECs, exposed to Au $\frac{1}{2}$ Ab under shear stress and flow conditions, made it impossible to quantify the uptake, since we could not determine which particles were inside the cell and which were merely attached to the extracellular side of the membrane. In addition, the optical properties of agglomerated AuNPs could also affect the quantification. Nevertheless, the association between Au $\frac{1}{2}$ Ab and TNF-activated HUVECs was dramatically larger after shear stress adaptation and flow exposure conditions as compared with static conditions. Flow

cytometry data showed significantly increased SSC-A in TNF-activated HUVECs exposed to Au $\frac{1}{2}$ Ab under flow conditions compared with TNF-activated HUVECs exposed to Au $\frac{1}{2}$ Ab under static conditions (Fig. S8 in the ESI[†]).

ICAM-1 and PECAM-1 surface expression and AuNP-uptake

The surface expression of ICAM-1 and PECAM-1 on HUVECs was measured by flow cytometry after 3 h AuNP exposure ($5 \mu\text{g ml}^{-1}$) of cells that were cultured and exposed under static conditions or adapted to shear stress and exposed under flow conditions (Fig. 6). ANOVA was performed on results from the static conditions. The results for the shear stress adapted and flow exposed cells were analysed by separate Student's *t*-tests because the variation between static exposed and shear stress adapted and flow exposed cells was significantly different (Levene's test). The difference in variation is likely due to the reduced counts obtained by flow cytometry for the shear stress and flow exposed cells (1000–3000 counts) as compared with the static exposed cells (8000–10 000 counts).

We found increased ICAM-1 surface-expression for unexposed TNF-activated cells compared with the unexposed non-activated cells under static conditions as expected (33.4-fold, $P < 0.001$). High levels of ICAM-1 surface expression were also

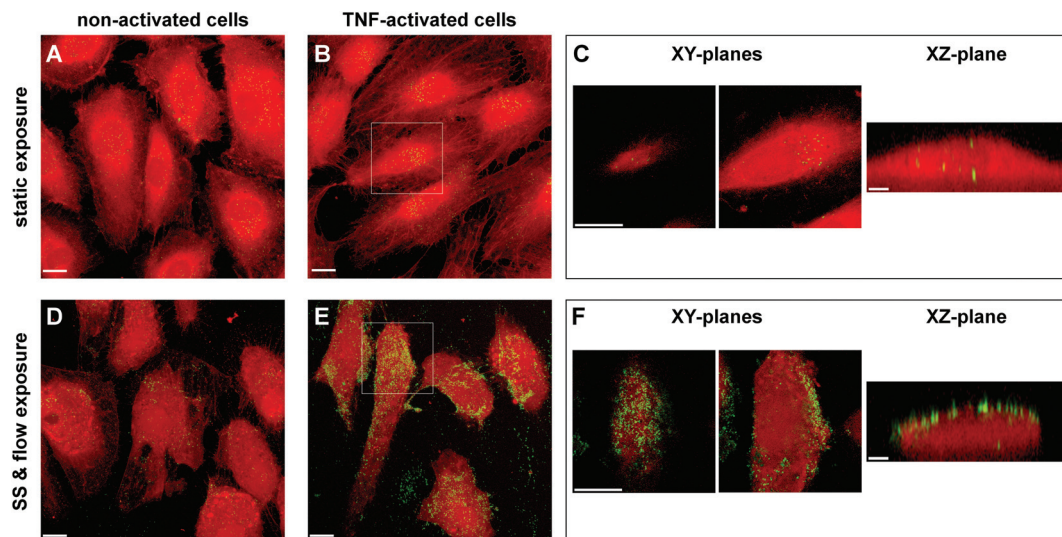


Fig. 5 Effects of shear stress (SS) adaptation and flow exposure on the association between anti-ICAM-1 antibody conjugated gold nanoparticles ($\text{Au}_{1/2}\text{Ab}$) and HUVECs. Cells were either non-activated or activated with TNF (24 h and 10 ng ml^{-1}) followed by exposure to AuNPs conjugated with cleaved anti-ICAM antibodies ($\text{Au}_{1/2}\text{Ab}$) ($5 \mu\text{g ml}^{-1}$ for 3 h) under either flow or static conditions. All cells exposed under flow conditions were SS adapted for 24 h (10 dyn) prior to $\text{Au}_{1/2}\text{Ab}$ exposure. Panels A and B show extended focus images of image-stacks of non-activated cells (A) and TNF-activated cells (B) exposed to $\text{Au}_{1/2}\text{Ab}$ under static conditions. Panel C shows two selected XY image planes and a rendered perpendicular XZ image plane of the region of interest (white box) in panel B. Panels D and E show extended focus images of image-stacks of non-activated cells (D) and TNF-activated cells (E) exposed to $\text{Au}_{1/2}\text{Ab}$ under flow conditions (after 24 h shear stress adaptation). Panel F shows two selected XY image planes and a rendered perpendicular XZ image plane of the region of interest (white box) in panel E. Images are representative of 3 independent experiments. Extended focus (A, B and D, E) and XY-plane scale bar = $14 \mu\text{m}$, XZ-plane scale bar = $3 \mu\text{m}$.

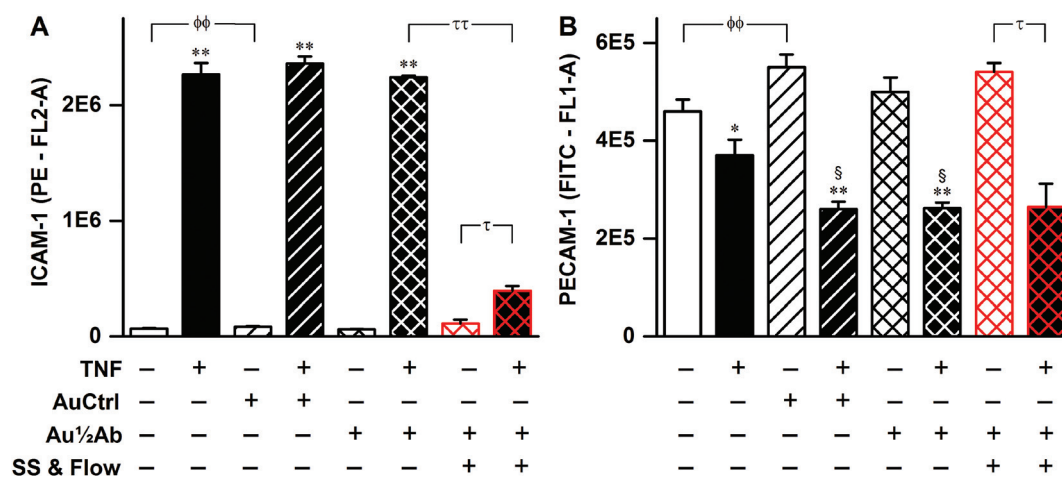


Fig. 6 Flow cytometry analysis of surface expression of ICAM-1 and PECAM-1 after gold nanoparticle (AuNP) exposure. Panels A and B show cell surface expression of ICAM-1 and PECAM-1, respectively. Shear stress-adapted cells (24 h at 10 dyn) were exposed to AuNPs ($5 \mu\text{g ml}^{-1}$ for 3 h) under flow conditions (SS & flow) at 10 dyn . The reference condition was HUVECs that were pre-cultured and exposed to AuNPs under static conditions. Error bars represent SEMs of 5 independent experiments, except for the ICAM-1 measurement in TNF-exposed cells without AuNP exposure (second bar, $n = 4$) and for non-activated SS & flow (seventh bar, $n = 3$). * $P < 0.05$ and ** $P < 0.001$ compared with the non-activated corresponding AuNP exposure (ANOVA), § $P < 0.05$ compared with static TNF-activated unexposed cells (ANOVA), φ $P < 0.001$ (ANOVA), τ $P < 0.05$, ττ $P < 0.001$ (t-test).

observed for TNF-activated cells exposed to AuCtrl (27.6-fold, $P < 0.001$) and $\text{Au}_{1/2}\text{Ab}$ (37.2-fold, $P < 0.001$) under static conditions compared with non-activated cells with the same exposure conditions. In contrast, there was only a modest

increase in the ICAM-1 surface expression in the TNF-activated, shear stress adapted and $\text{Au}_{1/2}\text{Ab}$ flow exposed cells as compared with non-activated cells with the same exposure conditions (3.5-fold, $P < 0.05$). Collectively, this shows that there is

less ICAM-1 signals on the surface of Au $\frac{1}{2}$ Ab exposed cells under flow conditions as compared with static conditions. This could be due to the increased binding of Au $\frac{1}{2}$ Ab to the ICAM-1 receptor on the cell surface. Thus, steric hindrance of the ICAM-1, by binding to Au $\frac{1}{2}$ Ab, blocks the detection of the receptor by flow cytometry.

The surface-expression of PECAM-1 was significantly lower for unexposed TNF-activated cells compared with the non-activated cells under static conditions ($P < 0.05$). The PECAM-1 surface expression was further reduced in TNF-activated cells exposed to either AuCtrl or Au $\frac{1}{2}$ Ab under static conditions compared with unexposed TNF-activated cells ($P < 0.05$).

The cell size evaluated by forward scatter (FSC-A) showed an increased cell size for static unexposed TNF-activated cells and static AuCtrl-exposed cells (both activated and non-activated) as compared with static unexposed cells ($P < 0.05$). TNF-activated and shear stress-adapted cells after Au $\frac{1}{2}$ Ab exposure under flow conditions showed a significant reduction in the cell size ($P < 0.001$) (Fig. S8 in the ESI†).

Discussion

The effect of shear stress on the cellular uptake of NPs is of great importance in the development of intravenously delivered nanomedicine. Although AuNPs have been a widely-used model and drug-candidate NPs there has been no systematic study on the uptake of AuNPs under shear stress and flow conditions, the natural conditions in the circulatory system.

We found that shear stress adaptation and exposure to flow conditions reduced the uptake of unmodified AuNPs, which fits well with other experimental work showing reduced uptake of negatively charged fluorescent polystyrene NPs (100 nm) when human aortic endothelial cells (HAECs) were exposed to flow conditions (1 and 5 dyn, 30 min, not shear stress adapted).²⁹ Another study using immortalised HUVECs showed no uptake of negatively charged SiO $_2$ -NPs (50 nm) under static conditions, whereas there was increased uptake during a 20 min exposure under flow conditions in cells that were not shear stress adapted, although the exact NP localisation (intracellular, loosely associated or acellular) was not clearly described.³⁰

Most studies have not adapted the cells to shear stress before conducting the exposure to NPs under flow conditions. However, studies on uptake after only a short duration of flow exposure (15–30 min) indicate a different time-dependent uptake/association behaviour than static uptake behaviour as predicted by theoretical models on “particle margination” of NP-association to surfaces under flow conditions.³¹ The shear stress adaptation in our experiment (24 h) facilitated formation of stress fibres and other phenotypic changes in HUVECs, which might affect uptake behaviour. For instance, it has been hypothesized that endothelial cells, which were shear stress adapted for 24 h, had reduced uptake of ICAM-1 targeted polystyrene NPs (with a diameter of ~180 nm) because of the recruitment of the actin cytoskeleton to maintain the

cell shape, cell junctions and focal adhesion to the surface under flow.¹⁹ Other studies have demonstrated reduced NP internalisation after 16 h of shear stress adaptation in HUVECs exposed to antibody conjugated anti-PECAM-NPs and similar reductions in NP internalisation were observed after inducing stress fibre formation by thrombin treatment.³² Furthermore, microarray analysis of HUVECs showed regulation of 52 genes after 6 h and 24 h of shear stress adaptation (25 dyn), among these down-regulations of caveolin-1 and α -tubulin (subunits of microtubules).⁸ Another microarray analysis of HAECs showed altered expression of 124 genes after 24 h of shear stress adaptation (12 dyn) among these down-regulations of caveolin-1 and alterations of 23 genes related to the cytoskeleton and the extracellular matrix (most of them down-regulated).⁷ This includes the expressional down-regulation of coronin-1A (coronin-like protein p57), which has been suggested to be directly involved in phagocytosis *via* interaction with Arp2/3 and F-actin in human neutrophils and in mouse RAW 264.7 macrophages.^{33,34} The uptake of AuCtrl and transferrin coated AuNPs has previously been suggested to be partly mediated by clathrin-mediated endocytosis,^{27,35} while poly(2-hydroxypropylmethacrylamide)-coated particles have been associated with the flotillin-dependent endocytotic pathway which is clathrin- and caveolae-independent.³⁶ The integrity of both clathrin- and flotillin-dependent endocytotic pathways has also been associated with F-actin and dynamic changes of the actin cytoskeleton.^{37,38} This, together with the increased recruitment of cytoplasmic globular actin for the F-actin stress fibre formation, may explain the reduced internalisation of AuNPs in HUVECs adapted to shear stress for 24 h.

We found that the Au $\frac{1}{2}$ Ab was internalised in activated HUVECs to a higher degree compared with non-activated HUVECs. This is to our knowledge the first time that targeted metallic NPs have been used in this context, whereas targeting of activated endothelial cells with anti-ICAM-1 polystyrene NPs has been studied for various sizes (0.18–10 μ m) and shapes in HUVECs and an endothelial-like cell line, EAhy926.^{14–17,19,39} In addition, anti-ICAM-1 antibody conjugated NPs showed increased passive adhesion after exposure at 4 °C or para-formaldehyde-fixation compared with unmodified polystyrene NPs.^{14,16,40} The pronounced increase of Au $\frac{1}{2}$ Ab internalisation in TNF-activated HUVECs can be explained by differences in the internalisation pathways of Au $\frac{1}{2}$ Ab and AuCtrl. As described earlier, the internalisation of AuNPs has been associated with both clathrin- and flotillin-dependent endocytosis.^{27,35,36} ICAM-1 conjugated NPs have in turn been suggested to be internalised by a clathrin- and caveolae-independent pathway, described as CAM-mediated endocytosis, which requires the clustering of ICAM-1 receptors.¹⁵ The confocal images indicated that both AuCtrl and Au $\frac{1}{2}$ Ab were localised together within vesicular structures, which is in agreement with our previous findings for 80 nm AuCtrl that was confirmed by focused ion beam-scanning electron microscopy (FIB-SEM).²⁷

The substantial increase in association between Au $\frac{1}{2}$ Ab and shear stress-adapted TNF-activated HUVECs under flow conditions is in agreement with the physiological role of ICAM-1

in the recruitment of leukocytes to activated endothelial cells.^{41,42} This may be related to a high number of receptors on the cell membrane because it has previously been shown that shear stress augmented TNF-induced ICAM-1 expression on endothelial cells.^{43,44} Theoretical models on the interaction between anti-ICAM-1 antibody-conjugated NPs and endothelial cells under shear stress conditions have described a shear-enhanced binding phenomenon with a threshold-limited enhancement of adhesion with increasing shear stress.^{45,46} The flow-mediated shear stress enhances stability of the receptor-ligand bindings until a threshold where the drag force exceeds that of the binding force, thereby promoting the detachment of anti-ICAM-1 NPs from the ICAM-1 receptors.⁴⁵ The multivalency (multiple molecular recognition events) of the binding between NPs and the cell surface (ICAM-1 receptors) is important for the adhesion of the anti-ICAM-1 NPs under flow conditions and can be maintained by having a high number of ligands (antigen-recognition sites) available on the NPs.⁴⁶ Other studies on anti-ICAM-1 NPs in shear stress-adapted cells and under flow conditions have not reported increased cell adhesion. For instance, anti-ICAM-1 polystyrene beads (~200 nm) exposed (15 min and 0–2 h, shear stress-adapted for 24 h) to TNF-activated HUVECs under flow conditions (4 dyn and 9 dyn) showed no difference in adhesion compared with static exposed TNF-activated cells.^{17,19} The uptake of anti-ICAM-1 paramagnetic liposomes (130–140 nm) was shown to be reduced with the increasing flow rate after 2 h exposure (0–5 dyn) in TNF-activated mouse brain endothelioma (bEnd.5) cells.²⁰ However, the quantification of the uptake did not appear to allow differentiation between surface adhesion and uptake, and cells were not distinguishable in the provided figures. The smaller size of our anti-ICAM-1 AuNPs may alter the dissociation from the cell's surface due to the reduced mechanical drag force on the NPs mediated by the flow. However, simulations indicate that a 200 nm anti-ICAM-1 NPs would have a slightly higher dissociation energy threshold than a 100 nm anti-ICAM-1 NPs due to a higher multivalency between the cellular ICAM-1 molecules and the NPs.⁴⁵ The difference in observed adhesion kinetics may also be due to different conjugation configurations. All the studies on anti-ICAM-1 NPs were conducted using full-length (intact) anti-ICAM-1 antibodies and random conjugation to the NPs, whereas cleaved antibodies can stabilise and orientate conjugation to the Au surfaces *via* the exposed native thiol functional groups, and thereby increase the likelihood of antigen–antibody binding.²¹ This also fits with the theoretical models on the dependency of maintaining the level of multivalent binding between anti-ICAM-1 antibodies on the NPs and cells above a certain threshold to facilitate adhesion during flow.^{45,46}

Effects of AuNP exposure on ICAM-1 and PECAM-1 surface expression have not been reported earlier to our knowledge. Increased surface expression of ICAM-1 on HUVECs has been associated with exposure to metallic NPs of similar size such as TiO₂ NPs (95 nm) and Al₂Si₂O₅(OH)₄ NPs (kaolinite aluminium silicate 30–75 nm) both related to a slight increase in

reactive oxygen species (ROS) production.⁴⁷ Previously, we have found a slight increase in ROS production in HUVECs exposed to 80 nm AuCtrl.²⁷ Non-metallic NPs have also been shown to increase both the ROS production and ICAM-1 surface expression in HUVECs after exposure to diesel exhaust particles and carbon black NPs.^{48,49} An increase in ROS production has been associated with increased ICAM-1 expression.⁵⁰ We also found that AuNP increased PECAM-1 expression, similar to the increase found after exposure to ~420 nm TiO₂ particle agglomerates and ambient air particulate matter.^{51,52} In contrast to ICAM-1, TNF exposure is known to reduce PECAM-1 surface expression and alter leukocyte transmigration *via* the involvement of intercellular junctions.⁵³ This was further reduced after exposure to AuNPs indicating that a cooperative effect with TNF as a slight increase in PECAM-1 surface expression was observed after AuNP exposure in non-activated cells.

Conclusions

Shear stress adaptation of HUVECs prior to AuNP exposure under flow conditions reduced the internalisation of AuNPs, whereas flow exposure conditions enhanced the association between anti-ICAM-1 AuNPs and TNF-activated shear stress-adapted HUVECs. This suggests that targeting of nano-carriers for leukocyte adhesion receptors will be particularly effective under flow conditions to shear stress-adapted endothelial cells.

Abbreviations

2-MEA	2-Mercaptoethylamine
AuNPs	Gold nanoparticles
AuCtrl	Unmodified AuNPs
AuAb	AuNPs modified with full length antibody against ICAM-1
Au $\frac{1}{2}$ Ab	AuNPs modified with cleaved antibody against ICAM-1
CLSM	Confocal laser scanning microscopy
FSC-A	Forward scatter
SSC-A	Side scatter

Acknowledgements

The study was supported by the Lundbeck Foundation Center for Biomembranes in Nanomedicine. We acknowledge the Center for Advanced Bioimaging (CAB) University of Copenhagen, Denmark where the (Perkin Elmer) Volocity 3D image analysis was conducted. Furthermore, we acknowledge the lending of equipment and technical instructions for the SDS-PAGE analysis by Peter Born Thodsen and Per Amstrup Pedersen at the Section for Molecular Integrative Physiology, Department of Biology, University of Copenhagen, Denmark.

References

- 1 W. C. Aird, in *Endothelial Biomedicine*, Cambridge University Press, New York, 2007, vol. 2007, pp. 227–229.
- 2 J. D. Kakisis, C. D. Liapis and B. E. Sumpio, *Endothelium*, 2004, **11**, 17–28.
- 3 T. Saxer, A. Zumbuehl and B. Muller, *Cardiovasc. Res.*, 2013, **99**, 328–333.
- 4 S. Pradhan and B. Sumpio, *Front. Biosci.*, 2004, **9**, 3276–3285.
- 5 N. Azuma, S. A. Duzgun, M. Ikeda, H. Kito, N. Akasaka, T. Sasajima and B. E. Sumpio, *J. Vasc. Surg.*, 2000, **32**, 789–794.
- 6 C. G. Galbraith, R. Skalak and S. Chien, *Cell Motil. Cytoskeleton*, 1998, **40**, 317–330.
- 7 B. P. Chen, Y. S. Li, Y. Zhao, K. D. Chen, S. Li, J. Lao, S. Yuan, J. Y. Shyy and S. Chien, *Physiol. Genomics*, 2001, **7**, 55–63.
- 8 S. M. McCormick, S. G. Eskin, L. V. McIntire, C. L. Teng, C. M. Lu, C. G. Russell and K. K. Chittur, *Proc. Natl. Acad. Sci. U. S. A.*, 2001, **98**, 8955–8960.
- 9 P. Decuzzi, R. Pasqualini, W. Arap and M. Ferrari, *Pharm. Res.*, 2009, **26**, 235–243.
- 10 T. L. Doane and C. Burda, *Chem. Soc. Rev.*, 2012, **41**, 2885–2911.
- 11 M. D. Howard, E. D. Hood, B. Zern, V. V. Shuvaev, T. Grosser and V. R. Muzykantov, *Annu. Rev. Pharmacol. Toxicol.*, 2014, **54**, 205–226.
- 12 J. S. Pober and W. C. Sessa, *Nat. Rev. Immunol.*, 2007, **7**, 803–815.
- 13 M. L. Dustin and T. A. Springer, *J. Cell Biol.*, 1988, **107**, 321–331.
- 14 S. Muro, C. Garnacho, J. A. Champion, J. Leferovich, C. Gajewski, E. H. Schuchman, S. Mitragotri and V. R. Muzykantov, *Mol. Ther.*, 2008, **16**, 1450–1458.
- 15 S. Muro, R. Wiewrodt, A. Thomas, L. Koniaris, S. M. Albelda, V. R. Muzykantov and M. Koval, *J. Cell Sci.*, 2003, **116**, 1599–1609.
- 16 S. Muro, E. H. Schuchman and V. R. Muzykantov, *Mol. Ther.*, 2006, **13**, 135–141.
- 17 S. Muro, T. Dziubla, W. Qiu, J. Leferovich, X. Cui, E. Berk and V. R. Muzykantov, *J. Pharmacol. Exp. Ther.*, 2006, **317**, 1161–1169.
- 18 A. J. Calderon, V. Muzykantov, S. Muro and D. M. Eckmann, *Biorheology*, 2009, **46**, 323–341.
- 19 T. Bhowmick, E. Berk, X. Cui, V. R. Muzykantov and S. Muro, *J. Controlled Release*, 2012, **157**, 485–492.
- 20 L. E. M. Paulis, I. Jacobs, N. M. van den Akker, T. Geelen, D. G. Molin, L. W. E. Starman, K. Nicolay and G. J. Strijkers, *J. Nanobiotechnol.*, 2012, **10**.
- 21 A. A. Karyakin, G. V. Presnova, M. Y. Rubtsova and A. M. Egorov, *Anal. Chem.*, 2000, **72**, 3805–3811.
- 22 E. C. Dreaden, A. M. Alkilany, X. Huang, C. J. Murphy and M. A. El-Sayed, *Chem. Soc. Rev.*, 2012, **41**, 2740–2779.
- 23 C. M. Cobley, J. Chen, E. C. Cho, L. V. Wang and Y. Xia, *Chem. Soc. Rev.*, 2011, **40**, 44–56.
- 24 E. Boisselier and D. Astruc, *Chem. Soc. Rev.*, 2009, **38**, 1759–1782.
- 25 J. A. Webb and R. Bardhan, *Nanoscale*, 2014, **6**, 2502–2530.
- 26 T. Tolker-Nielsen and C. Sternberg, in *Curr. Protoc. Microbiol.*, John Wiley & Sons, Inc., 2011, ch. 1, p. Unit 1B 2.
- 27 H. Klingberg, L. B. Oddershede, K. Loeschner, E. H. Larsen, S. Loft and P. Møller, *Toxicol. Res.*, 2015, **4**, 655–666.
- 28 R. J. Stewart, T. S. Kashour and P. A. Marsden, *J. Immunol.*, 1996, **156**, 1221–1228.
- 29 A. Lin, A. Sabnis, S. Kona, S. Nattama, H. Patel, J. F. Dong and K. T. Nguyen, *J. Biomed. Mater. Res., Part A*, 2010, **93**, 833–842.
- 30 S. P. Samuel, N. Jain, F. O'Dowd, T. Paul, D. Kashanin, V. A. Gerard, Y. K. Gun'ko, A. Prina-Mello and Y. Volkov, *Int. J. Nanomed.*, 2012, **7**, 2943.
- 31 P. Decuzzi, S. Lee, B. Bhushan and M. Ferrari, *Ann. Biomed. Eng.*, 2005, **33**, 179–190.
- 32 J. Han, B. J. Zern, V. V. Shuvaev, P. F. Davies, S. Muro and V. Muzykantov, *ACS Nano*, 2012, **6**, 8824–8836.
- 33 M. Yan, R. F. Collins, S. Grinstein and W. S. Trimble, *Mol. Biol. Cell*, 2005, **16**, 3077–3087.
- 34 M. Yan, C. Di Ciano-Oliveira, S. Grinstein and W. S. Trimble, *J. Immunol.*, 2007, **178**, 5769–5778.
- 35 B. D. Chithrani and W. C. Chan, *Nano Lett.*, 2007, **7**, 1542–1550.
- 36 C. Freese, R. E. Unger, R. C. Deller, M. I. Gibson, C. Brochhausen, H. A. Klok and C. J. Kirkpatrick, *Biomater. Sci.*, 2013, **1**, 824.
- 37 G. J. Doherty and H. T. McMahon, *Annu. Rev. Biochem.*, 2009, **78**, 857–902.
- 38 G. P. Otto and B. J. Nichols, *J. Cell Sci.*, 2011, **124**, 3933–3940.
- 39 S. Muro, M. Mateescu, C. Gajewski, M. Robinson, V. R. Muzykantov and M. Koval, *Am. J. Physiol.: Lung Cell. Mol. Physiol.*, 2006, **290**, L809–L817.
- 40 A. J. Calderon, T. Bhowmick, J. Leferovich, B. Burman, B. Pichette, V. Muzykantov, D. M. Eckmann and S. Muro, *J. Controlled Release*, 2011, **150**, 37–44.
- 41 L. Yang, R. M. Froio, T. E. Sciuto, A. M. Dvorak, R. Alon and F. W. Luscinskas, *Blood*, 2005, **106**, 584–592.
- 42 M. P. Burns and N. DePaola, *Am. J. Physiol.: Heart Circ. Physiol.*, 2005, **288**, H194–H204.
- 43 J. J. Chiu, P. L. Lee, C. N. Chen, C. I. Lee, S. F. Chang, L. J. Chen, S. C. Lien, Y. C. Ko, S. Usami and S. Chien, *Arterioscler., Thromb., Vasc. Biol.*, 2004, **24**, 73–79.
- 44 H. Methe, M. Balcells, M. del Carmen Alegret, M. Santacana, B. Molins, A. Hamik, M. K. Jain and E. R. Edelman, *Am. J. Physiol.*, 2007, **292**, H2167–H2175.
- 45 J. Liu, N. J. Agrawal, A. Calderon, P. S. Ayyaswamy, D. M. Eckmann and R. Radhakrishnan, *Biophys. J.*, 2011, **101**, 319–326.
- 46 J. Liu, G. E. R. Weller, B. Zern, P. S. Ayyaswamy, D. M. Eckmann, V. R. Muzykantov and R. Radhakrishnan, *Proc. Natl. Acad. Sci. U. S. A.*, 2010, **107**, 16530–16535.

- 47 L. Mikkelsen, K. A. Jensen, I. K. Koponen, A. T. Saber, H. Wallin, S. Loft, U. Vogel and P. Moller, *Nanotoxicology*, 2013, **7**, 117–134.
- 48 H. Frikke-Schmidt, M. Roursgaard, J. Lykkesfeldt, S. Loft, J. K. Nojgaard and P. Moller, *Toxicol. Lett.*, 2011, **203**, 181–189.
- 49 L. K. Vesterdal, L. Mikkelsen, J. K. Folkmann, M. Sheykhzade, Y. Cao, M. Roursgaard, S. Loft and P. Moller, *Toxicol. Lett.*, 2012, **214**, 19–26.
- 50 Y. Taniyama and K. K. Griendling, *Hypertension*, 2003, **42**, 1075–1081.
- 51 A. Montiel-Davalos, E. Alfaro-Moreno and R. Lopez-Marure, *Inhalation Toxicol.*, 2007, **19**(Suppl. 1), 91–98.
- 52 M. P. Ramos-Godinez, B. E. Gonzalez-Gomez, A. Montiel-Davalos, R. Lopez-Marure and E. Alfaro-Moreno, *Toxicol. In Vitro*, 2013, **27**, 774–781.
- 53 A. Woodfin, M. B. Voisin and S. Nourshargh, *Arterioscler., Thromb., Vasc. Biol.*, 2007, **27**, 2514–2523.